

Lattice expansion enables interstitial doping to achieve a high average ZT in n -type PbS

Zhengtao Liu¹ | Tao Hong² | Liqing Xu¹ | Sining Wang² | Xiang Gao³ | Cheng Chang⁴ | Xiangdong Ding¹ | Yu Xiao¹  | Li-Dong Zhao² 

¹State Key Laboratory for Mechanical Behavior of Materials, Xi'an Jiaotong University, Xi'an, China

²School of Materials Science and Engineering, Beihang University, Beijing, China

³Center for High Pressure Science and Technology Advanced Research (HPSTAR), Beijing, China

⁴Institute of Science and Technology Austria, Klosterneuburg, Austria

Correspondence

Yu Xiao, State Key Laboratory for Mechanical Behavior of Materials, Xi'an Jiaotong University, 710049 Xi'an, China. Email: xiao_yu@xjtu.edu.cn

Li-Dong Zhao, School of Materials Science and Engineering, Beihang University, 100191 Beijing, China. Email: zhaolidong@buaa.edu.cn

Funding information

National Science Fund for Distinguished Young Scholars, Grant/Award Number: 51925101; National Natural Science Foundation of China, Grant/Award Number: 52172236; Fundamental Research Funds for the Central Universities, Grant/Award Number: xtr042021007; Top Young Talents Programme of Xi'an Jiaotong University

Abstract

Lead sulfide (PbS) presents large potential in thermoelectric application due to its earth-abundant S element. However, its inferior average ZT (ZT_{ave}) value makes PbS less competitive with its analogs PbTe and PbSe. To promote its thermoelectric performance, this study implements strategies of continuous Se alloying and Cu interstitial doping to synergistically tune thermal and electrical transport properties in n -type PbS. First, the lattice parameter of 5.93 Å in PbS is linearly expanded to 6.03 Å in PbS_{0.5}Se_{0.5} with increasing Se alloying content. This expanded lattice in Se-alloyed PbS not only intensifies phonon scattering but also facilitates the formation of Cu interstitials. Based on the PbS_{0.6}Se_{0.4} content with the minimal lattice thermal conductivity, Cu interstitials are introduced to improve the electron density, thus boosting the peak power factor, from 3.88 $\mu\text{W cm}^{-1} \text{K}^{-2}$ in PbS_{0.6}Se_{0.4} to 20.58 $\mu\text{W cm}^{-1} \text{K}^{-2}$ in PbS_{0.6}Se_{0.4}-1%Cu. Meanwhile, the lattice thermal conductivity in PbS_{0.6}Se_{0.4}- $x\%$ Cu ($x=0-2$) is further suppressed due to the strong strain field caused by Cu interstitials. Finally, with the lowered thermal conductivity and high electrical transport properties, a peak $ZT \sim 1.1$ and $ZT_{\text{ave}} \sim 0.82$ can be achieved in PbS_{0.6}Se_{0.4}-1%Cu at 300–773K, which outperforms previously reported n -type PbS.

KEYWORDS

electrical transport properties, interstitial doping, PbS, thermal conductivity, ZT_{ave}

Zhengtao Liu and Tao Hong contributed equally to this study.

This is an open access article under the terms of the Creative Commons Attribution License, which permits use, distribution and reproduction in any medium, provided the original work is properly cited.

© 2023 The Authors. *Interdisciplinary Materials* published by Wuhan University of Technology and John Wiley & Sons Australia, Ltd.

1 | INTRODUCTION

Thermoelectric technology provides an effective route to solve energy and environmental issues because it is capable of directly converting heat into electricity.^[1–3] Nevertheless, its low efficiency and expensive price strongly limit its extensive applications. The conversion efficiency of thermoelectric material is closely related to the ZT value, $ZT = (S^2\sigma/\kappa)T$, where S , σ , κ , and T denote the Seebeck coefficient, electrical conductivity, thermal conductivity, and working temperature in Kelvin, respectively.^[4–6] Obviously, excellent thermoelectric materials are expected to own large S , high σ , and simultaneously low κ . But these contradictory transport relationships between carrier and phonon largely restrict thermoelectric performance.^[7,8]

Lead chalcogenides (PbQ, Q = Te, Se, and S) are excellent medium-temperature thermoelectric materials and have favorable carrier and phonon transport properties.^[9–15] Among lead chalcogenides, the earth-abundant PbS compound attracts increasing attention in the thermoelectric field. However, compared with high-performance PbTe and PbSe compounds, PbS presents a relatively low ZT value due to its strong atomic bond, which causes relatively low electrical transport and high thermal transport performance.^[16] Recent progress in PbS-based thermoelectric materials includes band sharpening to optimize carrier effective mass in n -type PbS–Sn–PbTe,^[17] composites to improve electron transport in n -type PbS,^[18,19] gap state and Fermi level pinning to maximize electrical performance in n -type PbS–Ga–In,^[20] microstructure engineering in PbS to reduce thermal conductivity,^[21–24] and so on. Notably, these works can only enhance the peak ZT value in PbS-based thermoelectric material at high temperatures, and its ZT_{ave} value still maintains an inferior level, which is mainly caused by the suppressed thermoelectric performance in the low-temperature range. Interestingly, Cu interstitial has been widely used to optimize the thermoelectric properties in PbTe and PbSe, especially near room temperature,^[25–28] and the synergy of covalent element alloying to intensify phonon scattering and Cu interstitial to boost carrier transport can largely enhance the ZT value at wide temperature range.^[29–31] However, compared with PbTe and PbSe systems, Cu doping in n -type PbS compound is difficult to form interstitials and plays an opposite role in tuning carrier transport properties.^[32] This different Cu role in n -type PbS is considered to be caused by its intrinsic low lattice space compared with PbSe and PbTe compounds.

To obtain high ZT_{ave} value in n -type PbS, this study firstly conducts heavily Se alloying to expand its lattice parameter, and then follows with Cu interstitial doping to simultaneously tune its electrical and thermal transport

properties. Results show that Se alloying can enhance the lattice parameter from 5.93 Å in PbS to 6.03 Å in PbS_{0.5}Se_{0.5}. This expanded lattice in Se-alloyed PbS can improve the solubility of Cu interstitials, thus boosting the electrical transport properties due to the optimized carrier density. The maximum power factor is largely enhanced from 3.88 $\mu\text{W cm}^{-1}\text{K}^{-2}$ in PbS_{0.6}Se_{0.4} to 20.58 $\mu\text{W cm}^{-1}\text{K}^{-2}$ in PbS_{0.6}Se_{0.4}–1%Cu. Owing to the strong mass fluctuation and strain field generated by heavy Se alloying and Cu interstitial doping, the lattice thermal conductivity is obviously lowered in PbS_{0.6}Se_{0.4}–1%Cu at a wide temperature range. Finally, with these simultaneously tuned electrical and thermal properties, the ZT_{ave} value in PbS_{0.6}Se_{0.4}–1%Cu can be boosted to 0.82 at 300–773K, which exceeds other high-performance n -type PbS samples and can also be comparable with some n -type PbSe- and PbTe-based thermoelectric materials.^[33–35]

2 | EXPERIMENTAL DETAILS

PbS-based samples were synthesized with the melting method and hot-pressing (OTF-1700X-RHP4) process to obtain highly densified bulk. Powder X-ray diffraction (PXRD) using Cu–K α radiation was employed to check phase composition. Microstructure observation was conducted with transmission electron microscopy (TEM) and scanning transmission electron microscopy (STEM). Hall coefficient (R_{H}) was measured by the van der Pauw method in Lake Shore 8400 Series at room temperature. The thermoelectric performance was evaluated with Cryoall CTA and LFA instruments. Experimental details can be found in Supporting Information.

3 | RESULTS AND DISCUSSION

3.1 | Lattice expansion in Se alloying in PbS_{1–x}Se_x ($x = 0–0.5$)

The PXRD results presented in Figure 1A indicate that all PbS_{1–x}Se_x ($x = 0–0.5$) samples have a cubic crystal structure, and Se alloying in PbS can form a complete solid solution up to $x = 0.5$. As Se atom (1.16 Å) has a larger atomic radius than that of the S atom (1.03 Å), the lattice parameter continuously increases with increasing Se alloying content in PbS_{1–x}Se_x ($x = 0–0.5$), from 5.93 Å in pure PbS to 6.03 Å in PbS_{0.5}Se_{0.5}, as shown in Figure 1B. The expanded lattice in PbS_{1–x}Se_x ($x = 0–0.5$) can provide larger space and make it possible to conduct interstitial doping in PbS-based thermoelectric material. Additionally, a large amount of Se alloying can cause strong mass fluctuation and strain field to scatter phonon

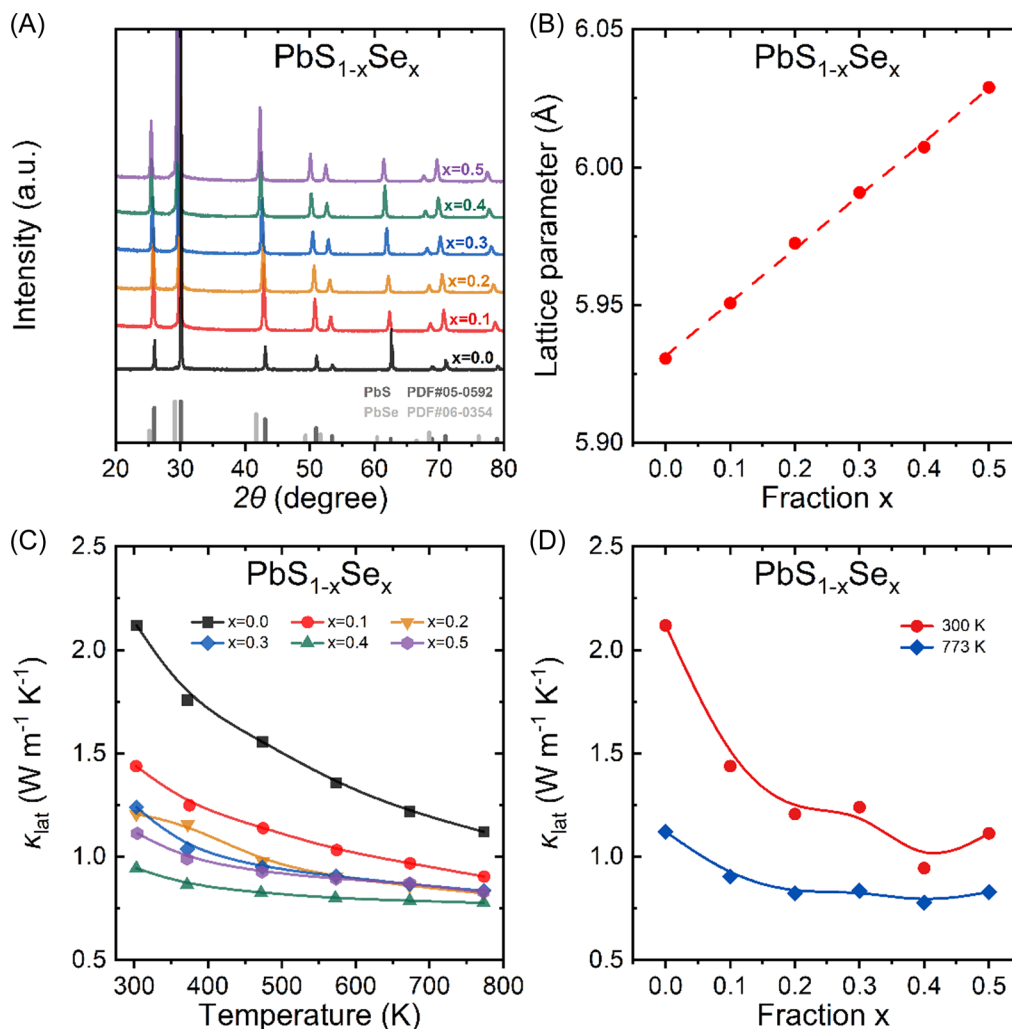


FIGURE 1 Phase identification and lattice thermal conductivity in $\text{PbS}_{1-x}\text{Se}_x$ (x = 0–0.5): (A) PXRD results, (B) the calculated lattice parameter, (C) temperature-dependent κ_{lat} , and (D) comparison of κ_{lat} values at 300 and 773 K.

so as to suppress the lattice thermal conductivity in the PbS matrix, as shown in Figure 1C. The lattice thermal conductivity in $\text{PbS}_{1-x}\text{Se}_x$ (x = 0–0.5) substantially decreases with increasing Se alloying content. And among $\text{PbS}_{1-x}\text{Se}_x$ (x = 0–0.5) samples, the $\text{PbS}_{0.6}\text{Se}_{0.4}$ sample presents the lowest κ_{lat} value in the entire temperature range. The κ_{lat} value is largely reduced from $2.12 \text{ W m}^{-1} \text{K}^{-1}$ in undoped PbS to $1.12 \text{ W m}^{-1} \text{K}^{-1}$ in $\text{PbS}_{0.6}\text{Se}_{0.4}$ at 300 K, and a large reduction of κ_{lat} value was also obtained at 773 K, from 0.94 to $0.78 \text{ W m}^{-1} \text{K}^{-1}$ in $\text{PbS}_{0.6}\text{Se}_{0.4}$ in Figure 1D. Notably, Se alloying in PbS not only intensifies phonon scattering but also causes extra scattering to carrier transport, therefore Se alloying leads to lowered electrical transport properties and no enhancement of ZT value is obtained in $\text{PbS}_{1-x}\text{Se}_x$ (x = 0–0.5), as shown in Supporting Information: Figure S1f. More detailed thermoelectric transport properties in $\text{PbS}_{1-x}\text{Se}_x$ (x = 0–0.5) can be found in Supporting Information: Figures S1 and S2.

3.2 | Cu interstitial doping to optimize electrical transport properties in $\text{PbS}_{0.6}\text{Se}_{0.4} - x\% \text{Cu}$ (x = 0–2)

The remarkable role of Cu interstitial doping to optimize thermoelectric properties has been widely proven in *n*-type PbSe and PbTe samples, but it presents negative impacts on thermoelectric performance in *n*-type PbS.^[32,36] As Cu atom can concurrently form both substitutions and interstitials in PbS, and the competing roles of Cu substitutions and interstitials in *n*-type PbS will deteriorate the carrier transport performance.^[32] In fact, the reason why Cu interstitials cannot be easily formed in PbS might originate from its small lattice parameter (5.93 Å) that cannot provide enough space for interstitials in the lattice. Therefore, this study conducts Cu interstitial doping in Se-alloyed PbS with expanded lattice, and Cu interstitial doping is based on $\text{PbS}_{0.6}\text{Se}_{0.4}$ content because it presents relatively low lattice thermal conductivity. Supporting

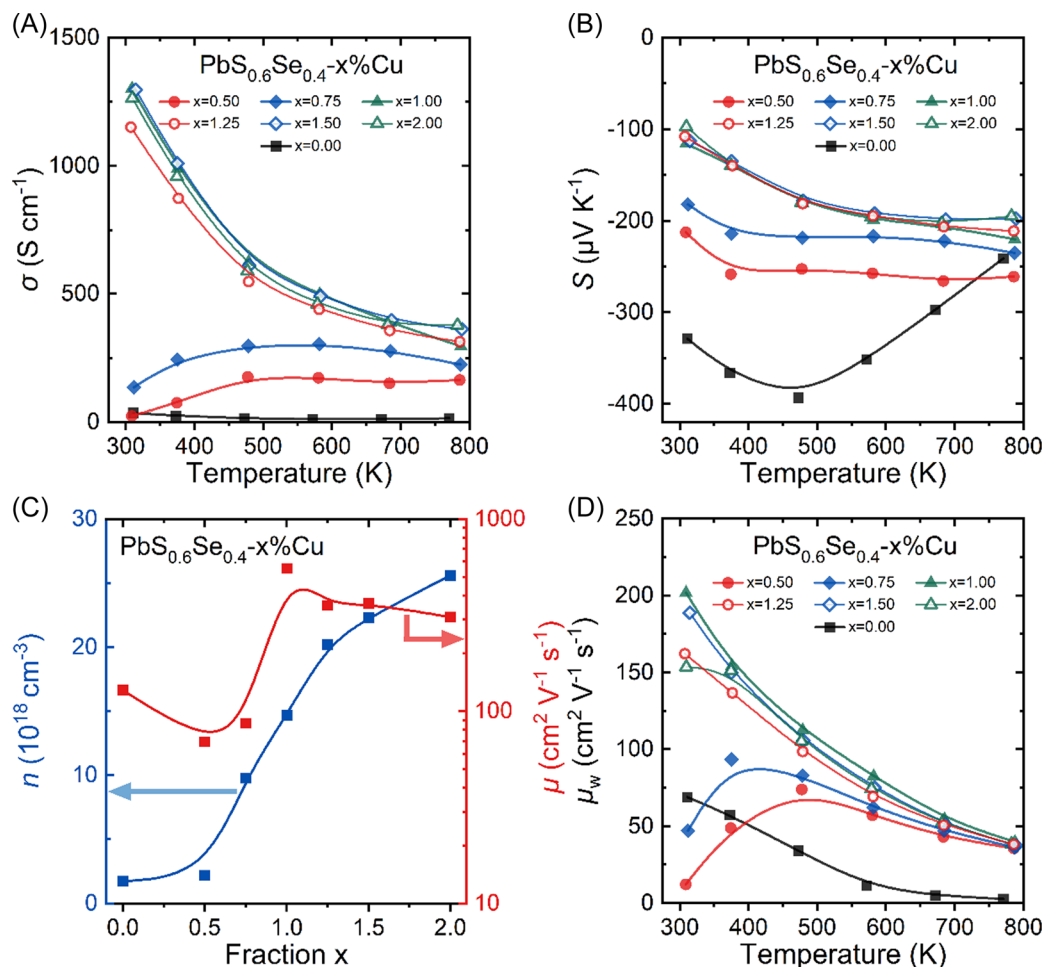


FIGURE 2 Electrical transport properties in $\text{PbS}_{0.6}\text{Se}_{0.4-x}\text{Cu}$ ($x = 0-2$): (A) electrical conductivity, (B) Seebeck coefficient, (C) hall carrier density and mobility at 300 K, and (D) weighted carrier mobility.

Information: Figure S3 presents the PXRD patterns of $\text{PbS}_{0.6}\text{Se}_{0.4-x}\text{Cu}$ ($x = 0-2$) and results suggest that all the Cu-doped $\text{PbS}_{0.6}\text{Se}_{0.4}$ samples still maintain cubic phase. The slight increase of lattice parameter with increasing Cu content implies the formation of interstitials in $\text{PbS}_{0.6}\text{Se}_{0.4}$ and the direct evidence of Cu interstitials will be introduced in the microstructure part.

Figure 2A presents that the electrical conductivity in $\text{PbS}_{0.6}\text{Se}_{0.4}$ is obviously improved after Cu interstitial doping, from 36 S cm^{-1} in $\text{PbS}_{0.6}\text{Se}_{0.4}$ to 1297 S cm^{-1} in $\text{PbS}_{0.6}\text{Se}_{0.4} - 1.5\% \text{Cu}$ at 300 K. With increasing Cu content, the temperature-dependent carrier transport properties incline to present degenerate-semiconductor transport behavior, which results from the optimized carrier density by Cu interstitial doping. Besides, the Seebeck coefficient in Cu-doped $\text{PbS}_{0.6}\text{Se}_{0.4}$ continuously decreases, as shown in Figure 2B, which is consistent with the improved electrical conductivity. Figure 2C shows the hall measurement results and demonstrates that the carrier density in $\text{PbS}_{0.6}\text{Se}_{0.4-x}\text{Cu}$ ($x = 0-2$) continuously increases with rising Cu content, from

$1.74 \times 10^{18} \text{ cm}^{-3}$ in $\text{PbS}_{0.6}\text{Se}_{0.4}$ to $2.56 \times 10^{19} \text{ cm}^{-3}$ in $\text{PbS}_{0.6}\text{Se}_{0.4} - 2\% \text{Cu}$ at 300 K. The largely increased carrier density comes from the released free carrier from Cu interstitials in $\text{PbS}_{0.6}\text{Se}_{0.4-x}\text{Cu}$ ($x = 0-2$). Correspondingly, the carrier mobility is well optimized in heavily Cu-doped $\text{PbS}_{0.6}\text{Se}_{0.4}$, which can be boosted to a maximum value of $553 \text{ cm}^2 \text{ V}^{-1} \text{ s}^{-1}$ in $\text{PbS}_{0.6}\text{Se}_{0.4} - 1\% \text{Cu}$ at room temperature. Notably, $\text{PbS}_{0.6}\text{Se}_{0.4-x}\text{Cu}$ ($x = 0, 0.5$, and 0.75) samples show relatively low carrier mobility at room temperature, which might be caused by interaction between majority and minority carriers in nondegenerate semiconductor.

Weighted carrier mobility (μ_w) is one of the most important parameters to evaluate carrier transport properties. To assess the role of Cu interstitials in $\text{PbS}_{0.6}\text{Se}_{0.4-x}\text{Cu}$ ($x = 0-2$), μ_w is calculated by S and σ with the following relationships^[17,37]:

$$\mu_w = \frac{3\sigma}{8\pi e F_0(\eta)} \left(\frac{h^2}{2m_e k_B T} \right)^{3/2}, \quad (1)$$

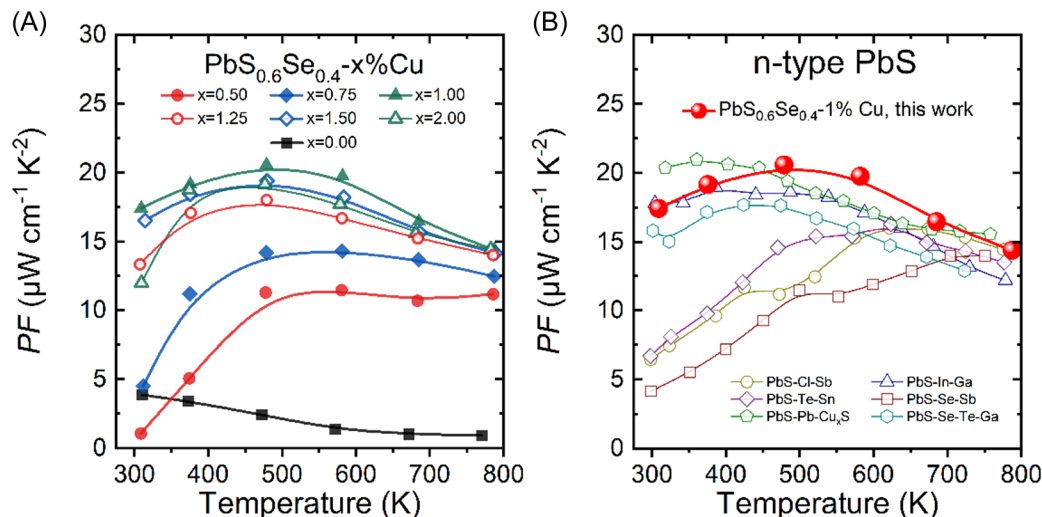


FIGURE 3 (A) Power factor in $\text{PbS}_{0.6}\text{Se}_{0.4}-x\%\text{Cu}$ ($x=0-2$), and (B) comparison of power factor in $\text{PbS}_{0.6}\text{Se}_{0.4}-1\%\text{Cu}$ and previous works, including PbS-Cl-Sb ,^[39] PbS-In-Ga ,^[20] PbS-Te-Sn ,^[17] PbS-Se-Sb ,^[21] $\text{PbS-Pb-Cu}_x\text{S}$,^[18] and PbS-Se-Te-Ga .^[22]

$$F_n(\eta) = \int_0^{\infty} \frac{x^n}{1 + e^{x-\eta}} dx, \quad (2)$$

$$S = \pm \frac{k_B}{e} \left(\frac{(r + 5/2)F_{r+2/3}(\eta)}{(r + 3/2)F_{r+1/2}(\eta)} - \eta \right), \quad (3)$$

where e , h , m_e , k_B , and r are the unit charge, Planck constant, electron mass, the Boltzmann constant, and scattering factor, respectively. When the acoustic scattering mechanism dominates, r equals $-1/2$.^[38] $F_n(\eta)$ is the Fermi integral and η is the reduced Fermi level. The calculated weighted carrier mobility in Cu interstitial doped- $\text{PbS}_{0.6}\text{Se}_{0.4}$ undergoes a large increase and the maximum μ_w achieves at $202 \text{ cm}^2 \text{ V}^{-1} \text{ s}^{-1}$ in $\text{PbS}_{0.6}\text{Se}_{0.4}-1\%\text{Cu}$ at 300 K, as shown in Figure 2D.

With the optimized carrier density and mobility after Cu interstitial doping in $\text{PbS}_{0.6}\text{Se}_{0.4}$, the power factor undergoes a remarkable increase at wide temperature. The peak power factor increases from $3.88 \mu\text{W cm}^{-1} \text{ K}^{-2}$ in $\text{PbS}_{0.6}\text{Se}_{0.4}$ to $20.58 \mu\text{W cm}^{-1} \text{ K}^{-2}$ in $\text{PbS}_{0.6}\text{Se}_{0.4}-1\%\text{Cu}$, as shown in Figure 3A, and the average power factor (PF_{ave}) in Supporting Information: Figure S4a undergoes substantial increase, from $2.01 \mu\text{W cm}^{-1} \text{ K}^{-2}$ in $\text{PbS}_{0.6}\text{Se}_{0.4}$ to $18.38 \mu\text{W cm}^{-1} \text{ K}^{-2}$ in $\text{PbS}_{0.6}\text{Se}_{0.4}-1\%\text{Cu}$ at 300–773 K. Compared with other n -type PbS, including PbS-Cl-Sb ,^[39] PbS-In-Ga ,^[20] PbS-Te-Sn ,^[17] PbS-Se-Sb ,^[21] $\text{PbS-Pb-Cu}_x\text{S}$,^[18] and PbS-Se-Te-Ga ,^[22] $\text{PbS}_{0.6}\text{Se}_{0.4}-1\%\text{Cu}$ in this study exhibits a superior power factor, as shown in Figure 3B, and also a highest PF_{ave} at 300–773 K as seen in Supporting Information: Figure S4b.

3.3 | Thermal conductivity and microstructure observation in $\text{PbS}_{0.6}\text{Se}_{0.4}-x\%\text{Cu}$ ($x=0-2$)

After Cu interstitial doping, the total thermal conductivity obtains a large increase in $\text{PbS}_{0.6}\text{Se}_{0.4}-x\%\text{Cu}$ ($x=0-2$), as shown in Figure 4A, which mainly arises from increased electronic thermal conductivity in Supporting Information: Figure S5c. On the contrary, the calculated lattice thermal conductivity in $\text{PbS}_{0.6}\text{Se}_{0.4}-x\%\text{Cu}$ ($x=0-2$) undergoes an obvious decrease after Cu interstitial doping, and the minimal κ_{lat} value decreases from $0.78 \text{ W m}^{-1} \text{ K}^{-1}$ in $\text{PbS}_{0.6}\text{Se}_{0.4}$ to $0.60 \text{ W m}^{-1} \text{ K}^{-1}$ in $\text{PbS}_{0.6}\text{Se}_{0.4}-2\%\text{Cu}$. With the roles of both Se alloying and Cu interstitial doping, the lattice thermal conductivity in $\text{PbS}_{0.6}\text{Se}_{0.4}-x\%\text{Cu}$ ($x=0-2$) is largely suppressed, and $\text{PbS}_{0.6}\text{Se}_{0.4}-1\%\text{Cu}$ owns the lowest lattice thermal conductivity. Figure 4B presents the lattice thermal conductivity of $\text{PbS}_{0.6}\text{Se}_{0.4}-1\%\text{Cu}$ to compare with other advanced n -type PbS samples, and results show that $\text{PbS}_{0.6}\text{Se}_{0.4}-1\%\text{Cu}$ exhibits comparably low lattice thermal conductivity, especially near room temperature. More detailed thermal properties of Cu-doped $\text{PbS}_{0.6}\text{Se}_{0.4}$ are provided in Supporting Information: Figure S5.

To unveil the origin of low lattice thermal conductivity in $\text{PbS}_{0.6}\text{Se}_{0.4}-1\%\text{Cu}$, scanning electron microscopy (SEM) and scanning transmission electron microscopy (STEM) are employed to disclose its structural features. The SEM result in Supporting Information: Figure S6a shows that no impurity phase exists in the matrix from microscale observation, which is consistent with its PXRD patterns. And the energy dispersive

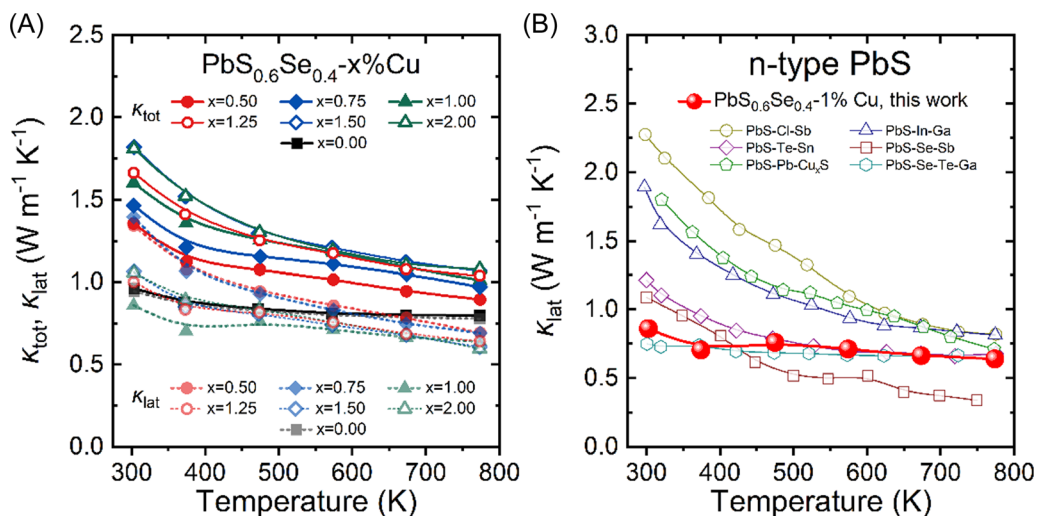


FIGURE 4 (A) Thermal conductivity in $PbS_{0.6}Se_{0.4-x}\%Cu$ ($x = 0-2$), and (B) comparison of lattice thermal conductivity between $PbS_{0.6}Se_{0.4}-1\%Cu$ and previous works, including $PbS-Cl-Sb$,^[39] $PbS-In-Ga$,^[20] $PbS-Te-Sn$,^[17] $PbS-Se-Sb$,^[21] $PbS-Pb-Cu_xS$,^[18] and $PbS-Se-Te-Ga$.^[22]

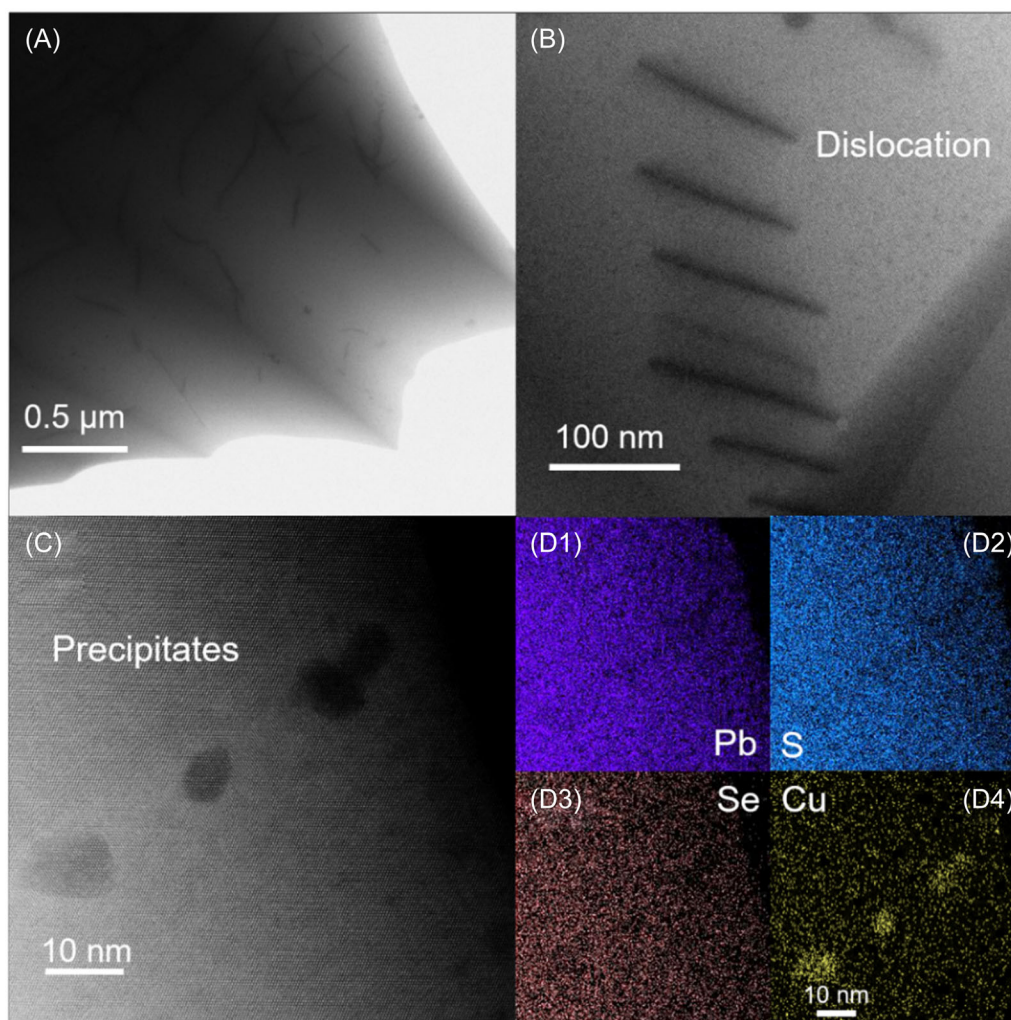


FIGURE 5 Microstructure observation in $PbS_{0.6}Se_{0.4}-1\%Cu$: (A) low-magnification STEM image, (B) dislocation in matrix, (C) annular dark-field (ADF) STEM image of the precipitates in $PbS_{0.6}Se_{0.4}$ matrix, and (D1–D4) EDS mappings of Pb, S, Se, and Cu elements.

spectroscopy (EDS) result proves all the elements distribute uniformly in the matrix, as shown in Supporting Information: Figure S6b. Some partial lines indicating dislocations are exhibited in the moderately magnified STEM image in Figure 5A. The dislocations are clearly visible in the larger magnification STEM image of Figure 5B. The precipitates are shown in the Annular dark-field (ADF) STEM image in Figure 5C and these Cu-rich nanoprecipitates vary from a few nanometers to a dozen nanometers. The corresponding EDS mapping results of Pb, S, Se, and Cu are shown in Figure 5D1–D4, respectively. Notably, the Cu element is locally enriched while the Pb, S, and Se elements are all homogeneously dispersed.

To clearly see the structural feature in Cu-rich precipitate, Cs-corrected STEM is carried out to look into its detailed atomic structure. The ADF image in Figure 6A shows a typical nanoprecipitate and the inset is its corresponding fast Fourier transform (FFT) image. The diffraction pattern is observed along [100] direction and proves that the crystal structure of the matrix is a cubic structure. Some extra weak diffraction spots marked by a dotted circle are also observed, implying different atomic structures in Cu-rich nanoprecipitate. The white box area is blacker than the other areas in the atomic resolution STEM image in Figure 6B, and

the enlarged atomic-resolved STEM image in Figure 6C proves the existence of Cu clusters in nanoprecipitates. These nanoscale clusters are composed of Cu interstitials and are widely distributed in a matrix, as shown in Figure 6D. The geometric phase analysis (GPA) results show a significant strain field around and inside the Cu clusters, and the strain field presents strong anisotropy along different strain tensors ϵ_{xx} and ϵ_{yy} , in Figure 6E,F. The microstructure observations in $\text{PbS}_{0.6}\text{Se}_{0.4}-1\%\text{Cu}$ disclose massive defects in different scales from atomic interstitial/clusters to nanoscale dislocations. And these small-size defects caused by Se alloying and Cu doping can intensify phonon scattering at high frequency and result in largely reduced lattice thermal conductivity.

3.4 | ZT value in $\text{PbS}_{0.6}\text{Se}_{0.4}-x\%\text{Cu}$ ($x=0-2$)

Cu interstitials have multiple functions and can simultaneously tune the electrical and thermal transport performance in $\text{PbS}_{0.6}\text{Se}_{0.4}-x\%\text{Cu}$ ($x=0-2$). Results prove that Cu interstitials can boost the value of $\mu_W/\kappa_{\text{lat}}$ at 300–700 K in Figure 7A, thus obviously enhancing the thermoelectric performance in Figure 7B. The ZT of 0.12

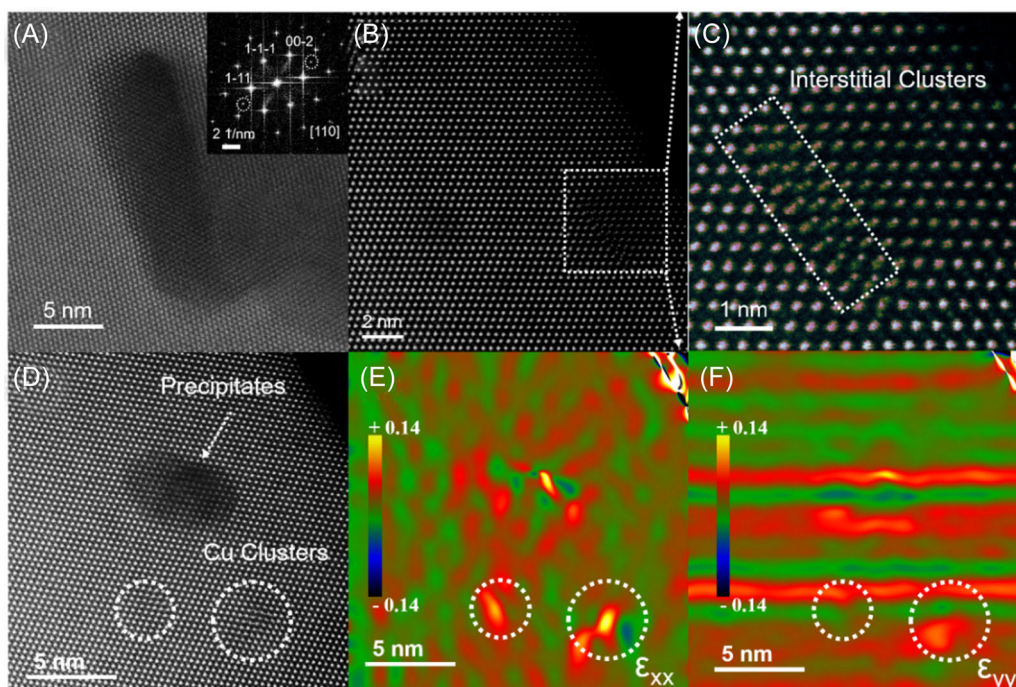


FIGURE 6 Atomic-defect observations in $\text{PbS}_{0.6}\text{Se}_{0.4}-1\%\text{Cu}$: (A) ADF STEM image of a typical nanoprecipitate, inset is its fast Fourier transform (FFT) image and shows the diffraction patterns of PbS matrix along [110] axis, (B) the high-angle annular dark field (HAADF) STEM image, (C) subtle atomic resolution image with Cu interstitial clusters, (D) atomic resolution STEM image with nanoprecipitate and Cu interstitial clusters, and (E–F) corresponding GPA strain analysis along horizontal (ϵ_{xx}) and vertical (ϵ_{yy}) directions.

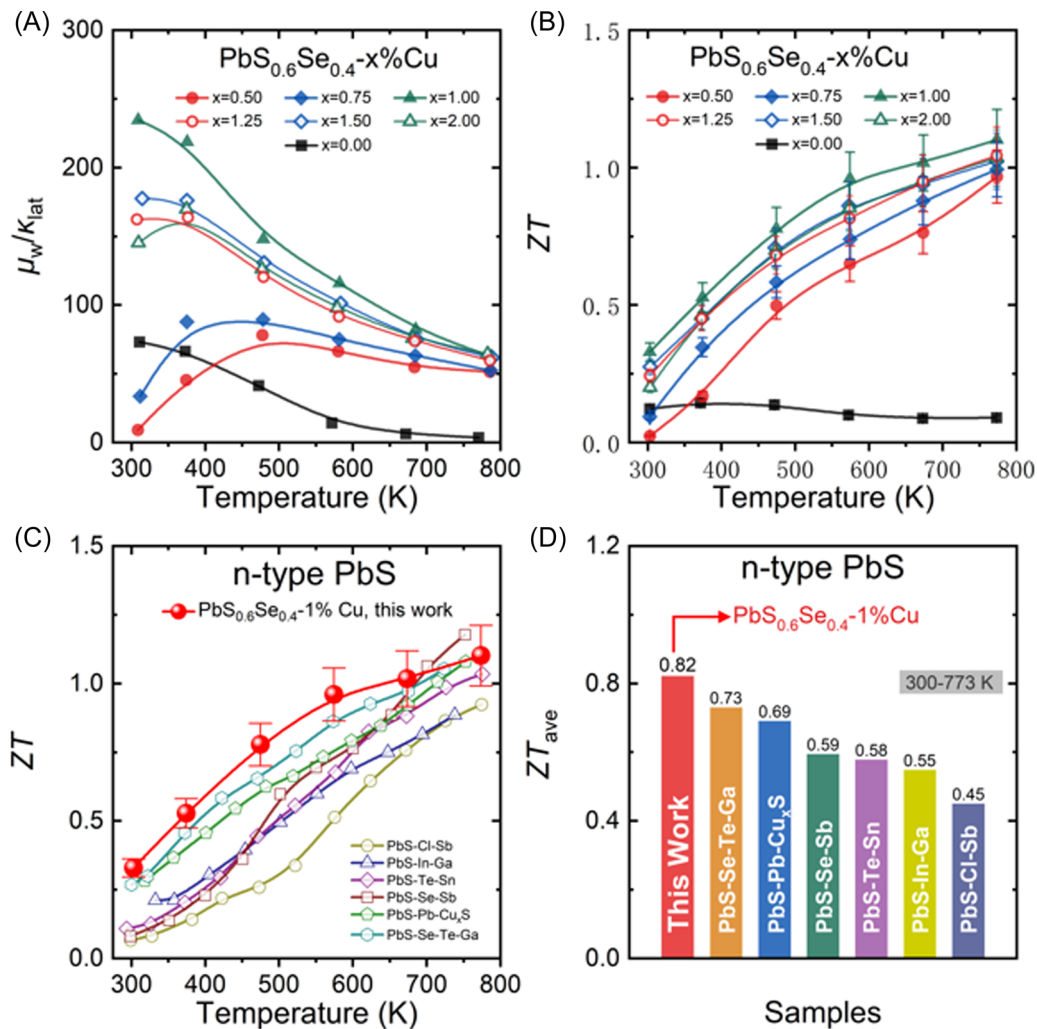


FIGURE 7 ZT value in $\text{PbS}_{0.6}\text{Se}_{0.4-x}\text{Cu}$ ($x = 0-2$): (A) $\mu_w/\kappa_{\text{lat}}$, (B) ZT value, comparisons of (C) ZT value and (D) ZT_{ave} value between $\text{PbS}_{0.6}\text{Se}_{0.4-1\%}\text{Cu}$ and other advanced n -type PbS, including PbS-Cl-Sb ,^[39] PbS-In-Ga ,^[20] PbS-Te-Sn ,^[17] PbS-Se-Sb ,^[21] $\text{PbS-Cu-Cu}_x\text{S}$,^[18] and PbS-Se-Te-Ga ^[22] at 300–773 K.

in $\text{PbS}_{0.6}\text{Se}_{0.4}$ is obviously improved to 0.3 in $\text{PbS}_{0.6}\text{Se}_{0.4-1\%}\text{Cu}$ at 300 K, and a maximum ZT value of 1.1 can also be obtained in $\text{PbS}_{0.6}\text{Se}_{0.4-1\%}\text{Cu}$ at 773 K. This largely enhanced wide-temperature thermoelectric performance in $\text{PbS}_{0.6}\text{Se}_{0.4-1\%}\text{Cu}$ makes it comparable with many previously reported n -type PbS samples in Figure 7C. A superior ZT_{ave} value of 0.82 can be finally achieved in $\text{PbS}_{0.6}\text{Se}_{0.4-1\%}\text{Cu}$ at 300–773 K, which outperforms other advanced n -type PbS at 300–773 K, including $ZT_{\text{ave}} \sim 0.73$ in PbS-Se-Te-Ga ,^[22] $ZT_{\text{ave}} \sim 0.69$ in $\text{PbS-Cu-Cu}_x\text{S}$,^[18] $ZT_{\text{ave}} \sim 0.59$ in PbS-Se-Sb ,^[21] $ZT_{\text{ave}} \sim 0.58$ in PbS-Te-Sn ,^[17] $ZT_{\text{ave}} \sim 0.55$ in PbS-In-Ga ,^[20] and $ZT_{\text{ave}} \sim 0.45$ in PbS-Cl-Sb ,^[39] as shown in Figure 7D. Notably, cycle tests and repeated experiments are also conducted, and results show that the high thermoelectric performance in $\text{PbS}_{0.6}\text{Se}_{0.4-1\%}\text{Cu}$ has good reproducibility and reliability as seen in Supporting Information: Figures S7–S9.

4 | CONCLUSIONS

In summary, a high ZT_{ave} of 0.82 can be achieved in $\text{PbS}_{0.6}\text{Se}_{0.4-1\%}\text{Cu}$ at 300–773 K. The enhanced thermoelectric performance at a wide temperature range is attributed to simultaneously optimized carrier and phonon transport properties by Se alloying and Cu interstitial doping. Se alloying can expand the lattice space so as to make it possible to form Cu interstitials in PbS matrix. Cu interstitial as donor dopant will release free carrier in $\text{PbS}_{0.6}\text{Se}_{0.4-1\%}\text{Cu}$, which can optimize the carrier density and largely improve its power factor in the whole temperature range. Moreover, Cu interstitial combination with Se alloying will cause a strong strain field in the $\text{PbS}_{0.6}\text{Se}_{0.4-1\%}\text{Cu}$ matrix to block phonon transport, thus substantially suppressing the thermal conductivity. This study successfully extends the strategy of interstitial doping to PbS-based thermoelectric

material and also further excavates its thermoelectric performance in low and medium temperature ranges.

AUTHOR CONTRIBUTIONS

Zhengtao Liu and Tao Hong contributed equally to this study. Zhengtao Liu synthesized the samples, conducted thermoelectric transport measurements, and drafted the manuscript; Tao Hong and Xiang Gao conducted the TEM observations and drafted the manuscript; Liqing Xu conducted thermal conductivity measurement, Sining Wang conducted Hall measurement, Cheng Chang and Xiangdong Ding revised the manuscript, Yu Xiao and Li-Dong Zhao conceived this study and revised the manuscript. All authors contributed to the discussions of the manuscript.

ACKNOWLEDGMENTS

The authors would like to acknowledge the strong support of microstructure observation from Center for High Pressure Science and Technology Advanced Research (HPSTAR). We acknowledge the financial support from the National Natural Science Foundation of China: 52172236, the Fundamental Research Funds for the Central Universities: xtr042021007, Top Young Talents Programme of Xi'an Jiaotong University and National Science Fund for Distinguished Young Scholars: 51925101.

CONFLICT OF INTEREST

The authors declare no conflict of interest.

ORCID

Yu Xiao  <http://orcid.org/0000-0003-3369-6852>

Li-Dong Zhao  <http://orcid.org/0000-0003-1247-4345>

REFERENCES

- [1] Tang X, Li Z, Liu W, Zhang Q, Uher C. A comprehensive review on Bi₂Te₃-based thin films: thermoelectrics and beyond. *Interdiscip Mater*. 2022;1(1):88-115.
- [2] Tan G, Zhao L-D, Kanatzidis MG. Rationally designing high-performance bulk thermoelectric materials. *Chem Rev*. 2016;116(19):12123-12149.
- [3] Liu W, Bai S. Thermoelectric interface materials: a perspective to the challenge of thermoelectric power generation module. *J Materiomics*. 2019;5(3):321-336.
- [4] Mao J, Liu Z, Zhou J, et al. Advances in thermoelectrics. *Adv Phys*. 2018;67(2):69-147.
- [5] Xiao Y. Routes to high-ranged thermoelectric performance. *Mater Lab*. 2022;1:220025.
- [6] Li C, Wu Y, Zhang Y-X, et al. Bi₂S₃ as a promising thermoelectric material: back and forth. *Mater Lab*. 2022;1:220014.
- [7] Liu Z. Challenges for thermoelectric power generation: from a material perspective. *Mater Lab*. 2022;1:220003.
- [8] Zhang F, Wu D, He J. The roles of grain boundaries in thermoelectric transports. *Mater Lab*. 2022;1:220012.
- [9] Jiang B, Yu Y, Chen H, et al. Entropy engineering promotes thermoelectric performance in p-type chalcogenides. *Nat Commun*. 2021;12(1):3234.
- [10] Jiang B, Yu Y, Cui J, et al. High-entropy-stabilized chalcogenides with high thermoelectric performance. *Science*. 2021;371(6531):830-834.
- [11] Zhang Q, Cao F, Liu W, et al. Heavy doping and band engineering by potassium to improve the thermoelectric figure of merit in p-type PbTe, PbSe, and PbTe_{1-y}Se_y. *J Am Chem Soc*. 2012;134(24):10031-10038.
- [12] Zheng W, Tan MF, Old LA, Paterson IC, Jakubovics NS, Choo SW. Subtle roles of Sb and S in regulating the thermoelectric properties of n-type PbTe to high performance. *Adv Energy Mater*. 2017;7(18):1700099.
- [13] Su X, Hao S, Bailey TP, et al. Weak electron phonon coupling and deep level impurity for high thermoelectric performance Pb_{1-x}Ga_xTe. *Adv Energy Mater*. 2018;8(21):1800659.
- [14] Zhao L-D, Wu HJ, Hao SQ, et al. All-scale hierarchical thermoelectrics: MgTe in PbTe facilitates valence band convergence and suppresses bipolar thermal transport for high performance. *Energy Environ Sci*. 2013;6(11):3346-3355.
- [15] Pei Y, Tan G, Feng D, et al. Integrating band structure engineering with all-scale hierarchical structuring for high thermoelectric performance in PbTe system. *Adv Energy Mater*. 2016;7(3):1601450.
- [16] Pei Y-L, Liu Y. Electrical and thermal transport properties of Pb-based chalcogenides: PbTe, PbSe, and PbS. *J Alloys Compd*. 2012;514:40-44.
- [17] Xiao Y, Wang D, Zhang Y, et al. Band sharpening and band alignment enable high quality factor to enhance thermoelectric performance in n-type PbS. *J Am Chem Soc*. 2020;142(8):4051-4060.
- [18] Li M, Liu Y, Zhang Y, et al. PbS-Pb-Cu_xS composites for thermoelectric application. *ACS Appl Mater Interfaces*. 2021;13(43):51373-51382.
- [19] Ibáñez M, Luo Z, Genç A, et al. High-performance thermoelectric nanocomposites from nanocrystal building blocks. *Nat Commun*. 2016;7:10766.
- [20] Luo Z-Z, Hao S, Cai S, et al. Enhancement of thermoelectric performance for n-type PbS through synergy of gap state and Fermi level pinning. *J Am Chem Soc*. 2019;141(15):6403-6412.
- [21] Jiang B, Liu X, Wang Q, et al. Realizing high-efficiency power generation in low-cost PbS-based thermoelectric materials. *Energy Environ Sci*. 2020;13(2):579-591.
- [22] Cheng R, Wang D, Bai H, et al. Bridging the miscibility gap towards higher thermoelectric performance of PbS. *Acta Mater*. 2021;220:117337.
- [23] Zhao L-D, He J, Hao S, et al. Raising the thermoelectric performance of p-type PbS with endotaxial nanostructuring and valence-band offset engineering using CdS and ZnS. *J Am Chem Soc*. 2012;134(39):16327-16336.
- [24] Zhao L-D, He J, Wu C-I, et al. Thermoelectrics with earth abundant elements: high performance p-type PbS nanostructured with SrS and CaS. *J Am Chem Soc*. 2012;134(18):7902-7912.
- [25] Xiao Y, Wu H, Li W, et al. Remarkable roles of Cu to synergistically optimize phonon and carrier transport in n-type PbTe-Cu₂Te. *J Am Chem Soc*. 2017;139(51):18732-18738.

- [26] You L, Liu Y, Li X, et al. Boosting the thermoelectric performance of PbSe through dynamic doping and hierarchical phonon scattering. *Energy Environ Sci.* 2018;11(7):1848-1858.
- [27] You L, Zhang J, Pan S, et al. Realization of higher thermoelectric performance by dynamic doping of copper in n-type PbTe. *Energy Environ Sci.* 2019;12(10):3089-3098.
- [28] Liu S, Yu Y, Wu D, et al. Coherent Sb/CuTe core/shell nanostructure with large strain contrast boosting the thermoelectric performance of n-type PbTe. *Adv Funct Mater.* 2021;31(5):2007340.
- [29] Xiao Y, Wu H, Shi H, et al. High-ranged ZT value promotes thermoelectric cooling and power generation in n-type PbTe. *Adv Energy Mater.* 2022;12(16):2200204.
- [30] Xiao Y, Xu L, Hong T, et al. Ultrahigh carrier mobility contributes to remarkably enhanced thermoelectric performance in n-type PbSe. *Energy Environ Sci.* 2022;15(1):346-355.
- [31] Xiao Y, Wu Y, Nan P, et al. Cu interstitials enable carriers and dislocations for thermoelectric enhancements in n-PbTe_{0.75}Se_{0.25}. *Chem.* 2020;6(2):523-537.
- [32] Zhao M, Chang C, Xiao Y, Gu R, He J, Zhao LD. Investigations on distinct thermoelectric transport behaviors of Cu in n-type PbS. *J Alloys Compd.* 2019;781:820-830.
- [33] Lee Y, Lo S-H, Chen C, et al. Contrasting role of antimony and bismuth dopants on the thermoelectric performance of lead selenide. *Nat Commun.* 2014;5:3640.
- [34] Qian X, Wu H, Wang D, et al. Synergistically optimizing interdependent thermoelectric parameters of n-type PbSe through introducing a small amount of Zn. *Mater Today Phys.* 2019;9:100102.
- [35] Xiao Y, Wu H, Wang D, et al. Amphoteric indium enables carrier engineering to enhance the power factor and thermoelectric performance in n-type Ag_nPb₁₀₀In_nTe_{100+2n} (LIST). *Adv Energy Mater.* 2019;9(17):1900414.
- [36] Qin Y, Hong T, Qin B, et al. Contrasting Cu roles lead to high ranged thermoelectric performance of PbS. *Adv Funct Mater.* 2021;31(34):2102185.
- [37] Snyder GJ, Snyder AH, Wood M, Gurunathan R, Snyder BH, Niu C. Weighted mobility. *Adv Mater.* 2020;32(25):2001537.
- [38] Pan L, Mitra S, Zhao L-D, et al. The role of ionized impurity scattering on the thermoelectric performances of rock salt AgPb_mSnSe_{2+m}. *Adv Funct Mater.* 2016;26(28):5149-5157.
- [39] Yang J, Zhang X, Liu G, et al. Multiscale structure and band configuration tuning to achieve high thermoelectric properties in n-type PbS bulks. *Nano Energy.* 2020;74:104826.

SUPPORTING INFORMATION

Additional supporting information can be found online in the Supporting Information section at the end of this article.

How to cite this article: Liu Z, Hong T, Xu L, et al. Lattice expansion enables interstitial doping to achieve a high average ZT in n-type PbS. *Interdiscip Mater.* 2023;2:161-170. doi:10.1002/idm2.12056